Sensors and Materials, Vol. 11, No. 3 (1999) 131–147
MYU Tokyo

S & M 0361

Thick Porous Silicon Thermo-Insulating Membranes

Piera Maccagnani, Renato Angelucci, Paolo Pozzi, Leonello Dori, Andrea Parisini, Marco Bianconi and Giuliana Benedetto*

CNR-LAMEL Institute, Via P. Gobetti 101, I-40129 Bologna, Italy
*Istituto Elettrotecnico Nazionale Galileo Ferraris, Strada delle Cacce 91, I-10135 Torino, Italy

(Received February 24, 1998; accepted February 18, 1999)

Key words: porous silicon, porous silicon oxidation, porous silicon nitridation, porous silicon membranes, dielectric membranes

A technological process aimed at realizing passivated porous silicon (PS) layers as the thermo-insulating material for thin as well as thick film gas sensor applications is reported and discussed. Oxidized PS (OPS) layers (5 to 35 μm thick) have been realized on p-Si substrates using the Si anodization process followed by PS thermal oxidation. The thick SiO_2 layer obtained from PS has the same stoichiometry as standard thermal silicon dioxide; unfortunately, stress introduced by the oxidation process induces significant wafer warpage, which inhibits further technological processing. Passivation of the PS layer can be achieved by a nitridation process executed in a rapid thermal system (RTS) in ammonia. In this case, the Si rods are covered by a thin oxynitride layer, which stabilizes the PS structure without introducing large stress. Nitrided PS membranes (25 – 30 μm thick) that are coplanar with the surrounding bulk Si and have good mechanical stability have been obtained.

1. Introduction

Since the early '90s, a new trend has characterized gas sensor technology. In fact, the increasing demand for miniature devices with low power consumption at high operating temperatures (≥ 400°C), and fabricated with IC-compatible technologies, has led to much effort aimed at realizing gas microsensors on silicon.

The results of those efforts are new devices based on bulk micromachined Si substrates with a very thin, suspended, dielectric membrane as the thermo-insulating material acting as the physical support of the entire sensor stack.[1] Other interesting works include the realization of a micro-hot plate on Si[2] using the surface micromachining technique. Despite these efforts, only thin-film technology can be used to deposit the sensing layer on different kinds of device structures. Unfortunately, most of the commercial gas sensor devices have a sensing layer realized using thick-film technology. With the aim of developing a standard low power consumption substrate heating element based on micromachined Si and useful for both thin- as well as thick-film gas sensor technology, porous silicon has been extensively investigated to replace the ultrathin suspended dielectric membrane as the thermo-insulating material and to act as a physical support of the sensor stack.

As is well known, PS has various morphologies, with a nano-, meso- or macro-porous structure. For the application we seek, PS with nano (1 – 10 nm) and meso-porous (10 – 50 nm) structures is the most interesting. In fact, in this PS material, thermal transport is low due to the very thin Si wall structure and to the presence of air inside the pores, which has very low thermal conductivity ($\approx$ 0.025 W/m·K).[3] Aside from this very interesting property, nano- and meso-PS materials are very difficult to process from a technological point of view. In fact, the PS structure is unstable when heated in an inert atmosphere.[4,5] As reported in refs. 4 and 5, heat treatments at temperatures between 300°C and 900°C lead to coarsening of the porous structure, that is, to an increase in pore size and in silicon rod thickness. The same authors explained that the PS structural changes are due to high surface energy associated with the very large surface area (200 – 300 m^2/cm^3) of the PS layer. Following this theory, the overall energy is decreased when thermal treatment is performed. In this case, the diffusion of silicon atoms takes place, which leads to pore aggregation; that is, larger pore radii and a smaller specific surface area. PS coarsening can be avoided if a thin SiO_2 layer is grown over the pore walls at low temperature. In this case, the grown SiO_2 film blocks the silicon atoms; thus, their diffusion is prevented. Therefore, PS needs to be "passivated" before undergoing any high-temperature process.

Another technological constraint associated with PS is its strong chemical reactivity to Si etchants used to realize the membranes. This further limits PS processability, and careful consideration is necessary in terms of process flow.

Taking into account the above considerations, a finite element method (SOLIDIS program, developed at ETH-Zurich[6]) is used to investigate the possibility of designing a new microstructure for gas sensor applications, including a PS layer as thermo-insulating material. This microstructure should exhibit, at the target temperature of 400°C, reduced power consumption (less than 150 mW) and low structure deformation. Simulations have shown that solutions based on a suspended membrane offer the most interesting thermal insulation properties, and that the insulation degree can be improved by reducing the membrane thickness or by increasing the membrane size. (Simulations have been performed by fixing the active area to 0.8×0.8 mm^2 and heating the microstructure with a double-spiral heater resistor). The structure of the selected microstructure is shown in Fig. 1.

As far as the PS layer in Fig. 1 is concerned, two different processing technologies have been considered. The first technology, reported in section 3, consists of the complete

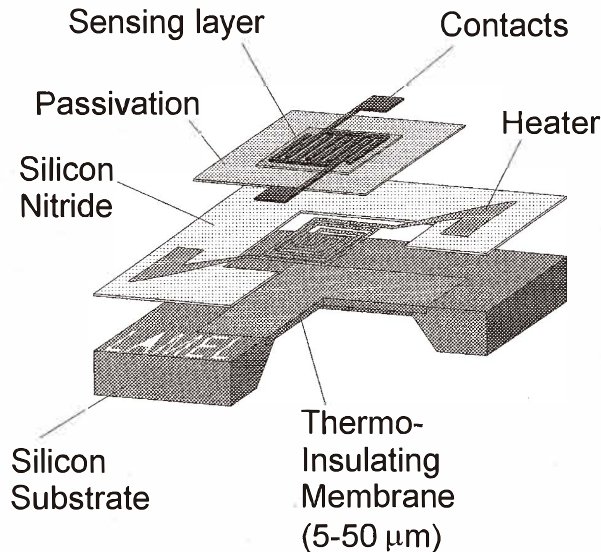

Fig. 1. Magnified view of micromachined Si structure.

conversion of the PS material into a compact SiO_2 layer whose thermal conductivity is well known (~ 1.4 W/m·K). This approach has been already investigated and the interesting results are published in ref. 7. The second one, reported in section 4, is characterized by growth of a thin Si_3N_4 film over the PS pore walls by exposing, at high temperatures, the PS structure to an ammonia (NH_3) atmosphere. In the latter case, the PS structure remains "open" and air fills the pores.

In the following, the experimental results related to the two technologies will be presented and discussed in view of the possibility of integrating them into the overall substrate heating element device technology.

2. Experimental

A p-type (100) Si substrate of 0.02 Ω·cm resistivity was used. To realize Si membranes several microns thick, bulk micromachining (Si etching from the back side of the wafer) with 40% in weight KOH solution at $T = 80°C$, was used. A 200 nm LPCVD Si_3N_4 masking layer protected the back side Si (outside the openings) during etching. The alignment between the openings on the back side of the wafer and the pattern defined on the front was realized using an IR-light converter, and double-side polished wafers were employed.

The Si anodization process was performed in a double electrochemical cell.[8] The porosity of the PS layers was 55% or 75%. The porosity values were obtained by changing the HF concentration and the anodization current density.

To selectively form the PS layer, two approaches were used:[9]
i) Si windows on selected wafer regions were opened by RIE in a LPCVD Si_3N_4 masking film. As well known, this film is characterized by good chemical inertness towards the HF anodic solution, but only for relatively short etching periods;
ii) selective PS formation is obtained taking advantage of the p^+ vs n^+ anodization selectivity.[9]

To oxidize PS and completely convert it into a compact SiO_2 layer, thermal treatments were performed in a standard oxidation furnace; the oxidation sequence was characterized by three major steps: the first one was executed in dry O_2 at $T = 300°C$, while the second and the third steps were executed in wet O_2 at $T = 850°C$ and $T = 1100°C$, respectively.

Partial nitridation of the porous Si structure was performed either in a standard furnace or in a rapid thermal system (RTS) in the temperature range between 1000 and 1100°C. Depending on the equipment in which the process was performed, the nitridation time varied from 2 to 30 min.

To evaluate stress magnitude at the border and inside the PS windows, X-ray topography analysis was performed. Cross sectional TEM observations were carried out to estimate: i) the Si anodization depth inside membranes several microns thick; and ii) the PS structure obtained under different anodization conditions. The chemical composition of oxidized or nitrided PS layers was determined by the Rutherford backscattering spectroscopy (RBS) technique. Cross sections of PS and OPS layers were observed using a scanning electron microscope (SEM).

Finally, the thermal behavior of nitrided porous silicon membranes was evaluated by means of the photoacoustic (PA) technique.

3. Realization of a Substrate Heating Element with a Thick Oxidized Porous Silicon (OPS) Membrane as Thermo-Insulating Material

In terms of complete device realization, it is necessary to investigate several technological issues:

I. Selective silicon anodization
II. OPS layer formation
III. OPS membrane release

A p-type (100) Si wafer of 0.02 Ω·cm resistivity was used as substrate. Si anodization was performed only on selected areas, using a 25% HF ethanoic solution and with a current density of 70 mA/cm^2. Selective PS formation was obtained taking advantage of the p^+ vs n^+ anodization selectivity or using an LPCVD Si_3N_4 layer as masking film. The anodization conditions, together with the average gravimetric porosity[10] and the PS layer thickness (obtained by SEM images of cross-sectional PS structures) are listed in Table 1. (For detailed information about the anodization process, see ref. 11).

In this section, we will focus attention on PS oxidation and OPS membrane release.

3.1 *PS oxidation*

After PS is formed, thermal treatment in an oxidizing ambient is necessary to convert PS into a compact OPS layer characterized by chemical inertness and high mechanical

Table 1
Anodization conditions used to grow PS layers of different thicknesses on heavily doped p-type Si.

Sample	J_{ps} (mA/cm^2)	Porosity (%)	$t_{anodization}$ (s)	Th_{ps} (μm)
ST3-1	70	55	90	5
ST3-2	70	55	360	24
ST2-5	70	57	600	38

stability, and having the thermal insulating properties characteristic of SiO_2. The oxidation time necessary to convert the PS layer into SiO_2 is not a function of PS thickness. In fact, oxygen diffuses into the entire PS film, and oxidation involves the entire volume of the PS layer. This allows the formation of an OPS layer with a thickness of 50 μm or more in around 2 hours. As specified in section 2, the oxidation process consists of three major steps. First, a very low temperature thermal treatment in dry O_2 is performed to grow a few SiO_2 monolayers and to avoid PS coarsening. Then, the oxidation step at T = 850°C in wet O_2 follows. After this step, the PS layer still has a certain amount of porosity left, which makes the PS structure fairly weak when it comes in contact with a HF or a KOH solution. This fact has a serious impact on the process flow, because OPS membranes with a porous structure cannot be formed by etching Si from the back side using a KOH solution. Therefore, to obtain suspended OPS membranes, two alternatives are available:

i) Perform a densification step at high temperature (~ 1100°C), which transforms the porous OPS layer into a compact SiO_2 film. The densified OPS layer is similar, in terms of chemical inertness, towards KOH, and of dissolution rate in HF solution, to SiO_2 obtained by thermal oxidation of Si. Densification is achieved by occurrence of the viscous flow of silica and requires a temperature higher than 1000°C. In our case, a third step at 1100°C in a wet O_2 ambient for 30 min was carried out. The surface and in-depth chemical compositions of this OPS layer were evaluated using either RBS or the energy dispersion spectroscopy (EDS). The in-depth chemical composition was obtained by removing a few microns (~20 μm) of the OPS layer each time. Both techniques confirmed the SiO_2 stoichiometry of the OPS layer. In Fig. 2, the RBS spectra of a densified OPS layer are shown.

ii) The other alternative requires the formation of a Si membrane of the desired thickness, realizing at first Si membranes of the desired thickness, and then executing selective anodization of the Si membranes, followed by the thermal oxidation sequence as specified above, but without the step at the highest temperature (1100°C).

Unfortunately, in both alternatives, the OPS membranes are strongly affected by a large stress generated by the thick SiO_2 layer grown. In particular, following the process reported in i), wafers with hundreds of PS windows (2.2 mm by side and 5 to 35 μm thick) were fully oxidized and densified at high temperature. A SEM micrograph of a cross-sectional window, 1 × 1 mm^2 in size and with the OPS layer 35 μm thick, is shown in Fig. 3. As reported in Table 2, all the patterned wafers with hundreds of PS windows show

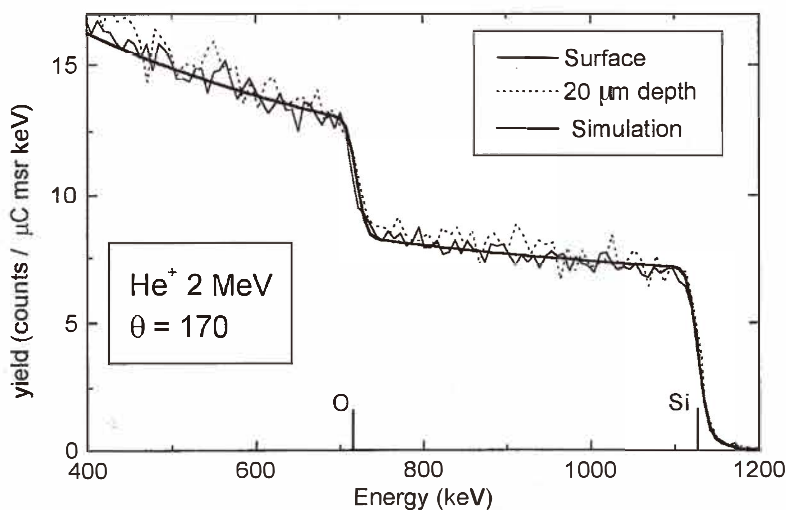

Fig. 2. RBS spectra of an OPS sample, taken at the surface and at 20 μm depth, compared with the simulation spectrum of an ideal SiO_2 film.

significant wafer warpage after the oxidation process. As other authors have already shown,[12] this warpage is due to the difference in the thermal expansion coefficient of Si and SiO_2, which leads to the generation of compressive stress. As a result of the warpage, the possibility of further processing exists only for the wafers with the 5-μm-thick OPS layers.

3.2 *OPS membrane release*

Another problem associated with the technological approach reported in the previous section, item i), occurs when the membranes are released. This step is accomplished by performing first a front-to-back wafer alignment, then an RIE etching of the masking layer (Si_3N_4) on selected areas, followed by Si etching using KOH solution (T = 80°C, [KOH] = 40% in weight). The final stages of the OPS membrane formation are schematically shown in Fig. 4 and can be described as follows: as soon as the Si thickness underneath the OPS layer is reduced, the high intrinsic stress associated with the thick oxide layer further increases the membrane warpage (Fig. 4(b)); with the membrane being curved, silicon etching by KOH does not proceed uniformly across the exposed surface, and portions of the OPS membrane all along the membrane border are disclosed (Fig. 4(c)). When the compressive stress of the OPS layer is no longer compensated by the presence of the bulk silicon layer, the membrane warps markedly and breaks (Fig. 4(d)).

The membrane release problem was solved following the processing step sequence reported in the previous section at item ii). Anyway, in spite of the mild oxidation process applied to the PS membrane (the maximum temperature was 850°C in wet ambient), the

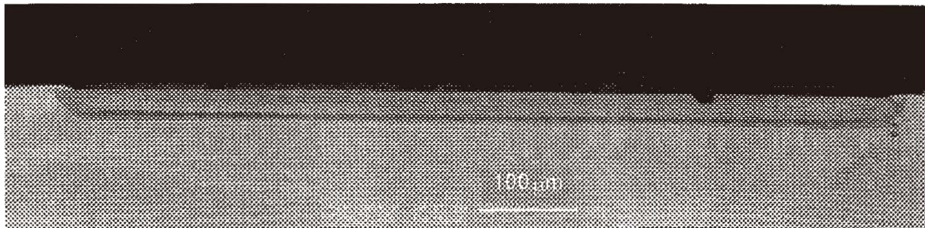

Fig. 3. SEM cross-sectional image of 1×1 mm^2 in size and 35-μm thick OPS layer grown on 0.02 Ω·cm p-type silicon, with n^+ implanted region as a masking layer.

Table 2
Wafer warpage obtained for wafers patterned with hundreds of OPS windows, as a function of OPS thickness.

Sample	OPS thickness (μm)	Wafer warpage (μm)
ST2-2	33	1914
ST2-5	33	1750
ST3-2	20	942
ST2-4	5	44
ST3-1	5	49

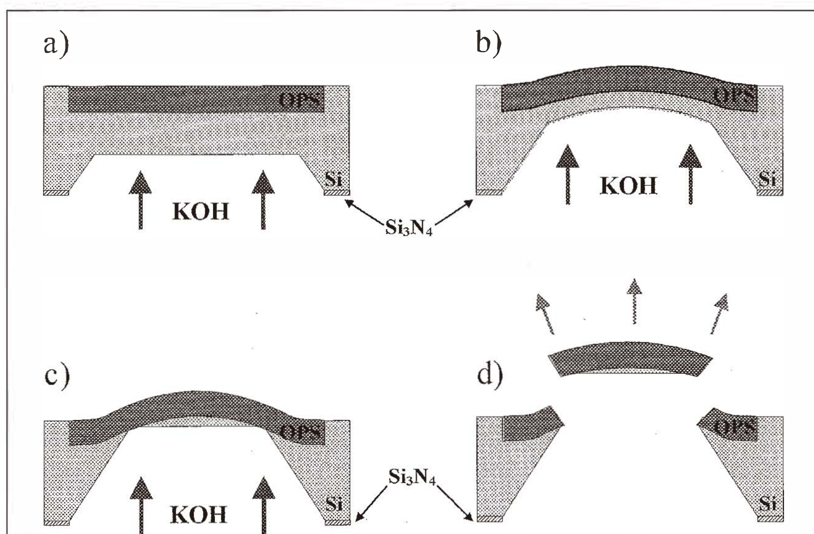

Fig. 4. Sketch of OPS membrane release during etching of silicon from the back of the wafer.

intrinsic stress generated during the thermal oxidation of PS was so high that the membranes assumed a blister-like shape, which prevents further wafer processing.

In summary, the stabilization of PS based on its thermal conversion into SiO_2, has shown technological constraints that limit the implementation of this step inside a standard process. In fact, PS oxidation causes marked wafer warpage, breaking up membranes during their release while etching Si from the back side, and formation of membranes with a blister-like shape immediately after the cooling step from the oxidation temperature to room temperature. It's important to notice that the results on PS oxidation obtained in our work are in clear disagreement with those reported by Tabata.[7] At the present time, the reasons are not well understood, and more work is in progress.

With the goal of achieving a fully IC-compatible fabrication process to realize the device shown in Fig. 1 using a stable PS layer as thermo-insulating membrane, we investigated the stabilization of PS through its thermal nitridation in ammonia. The results of this approach are reported in the next section.

4. Realizations of Substrate Heating Element with a Thick Nitrided Porous Silicon (NPS) Membrane as Thermo-Insulating Material

The process flow to obtain passivated PS membranes cannot have KOH etching as the last step. In fact, the inertness of the nitrided PS layer in KOH solution would be required. Preliminary investigations of the inertness in KOH solution (25% in weight) of a PS layer previously nitrided in a rapid thermal system have shown that this material cannot be left inside the Si etching solution for more than 10 min (this is true for both porosity values, 55% and 75%). Therefore, the process flow was changed as follows:

I. Silicon membrane formation
II. Anodization of Si membrane
III. PS passivation and stabilization
IV. Complete device fabrication using IC-technology-compatible process steps

4.1 *Silicon membrane formation*

As far as the formation of Si membranes with reproducible thickness (in the range of 20 to 30 μm) is concerned, an optical method combined with the X-ray diffraction technique has been used in routine and calibration measurements, respectively. Uniform Si removal during bulk Si etching was achieved using a 40% (in weight) concentrated KOH solution at 80°C, under constant stirring. Excellent results were obtained in terms of either membrane thickness uniformity over the entire wafer surface or the absolute membrane thickness value.

4.2 *Anodization of the Si membrane*

Anodization was executed on an area 2 cm in diameter, which included 9 square membranes 1.5 mm per side. Two porosity values were selected, namely, 55% and 75%. The 75% porosity value was chosen to improve thermal insulation properties[13] (no more being necessary to compensate for the volume expansion that follows Si oxidation), while maintaining good processing capability. The Si anodization conditions to obtain a PS layer

with 55% porosity are given in section 3. For formation of a PS layer of 75% porosity on a Si substrate of 0.02 Ω·cm resistivity, HF concentration in the electrochemical solution and anodization current density, J, were reduced, respectively, to 15% and 40 mA/cm^2. Under the reported conditions, the anodization rates were 5.27 μm/min and 2.15 μm/min, respectively, for 55% and 75% porosity.

A typical plot of the cell potential vs. time during the anodization process is shown in Fig. 5. In this case, the membrane thickness was 29 μm. The cell potential, whose trend with time does not depend on the porosity value, shows an initial, abrupt increase for about 15 s, and then it stabilizes. The time t_a at which anodization is assumed to reach the bottom of the Si membrane is determined by the sudden decrease in the electrode potential. Although anodization time longer than t_a is used, to take into account possible variations of Si membrane thickness, TEM observations of cross-sectional PS membranes (Figs. 6(a) and 6(b)) have revealed that a very thin nonanodized Si layer (100 – 200 nm thick) still exists at the bottom of the membrane. Finite element method (FEM) simulations of the thermal behavior of the microstructure, as a function of Si layer thickness in the PS membrane, have shown that the device power consumption at the highest sensor working temperature should not consistently increase owing to the presence of the residual Si layer (Table 3).

In Figs. 6(a) and 6(b), we note that there is no clear evidence of morphological differences between the PS layer with 55% porosity (Fig. 6(a)) and that with 75% porosity (Fig. 6(b)). In both cases, pore size and Si wire dimensions in the range of 10 – 20 nm are observed. However, the corresponding electron diffraction patterns shown in Figs. 7(a) and 7(b) reveal different features. Whereas the electron diffraction pattern of the 55% porosity sample (Fig. 7(a)) is similar to that of perfect bulk Si, the pattern of the 75%

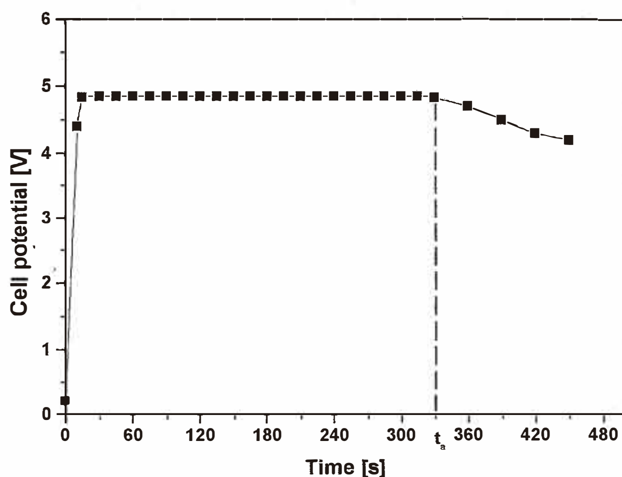

Fig. 5. Typical potential vs time curve during p-type silicon (0.02 Ω·cm) membrane (29 μm thick) anodization.

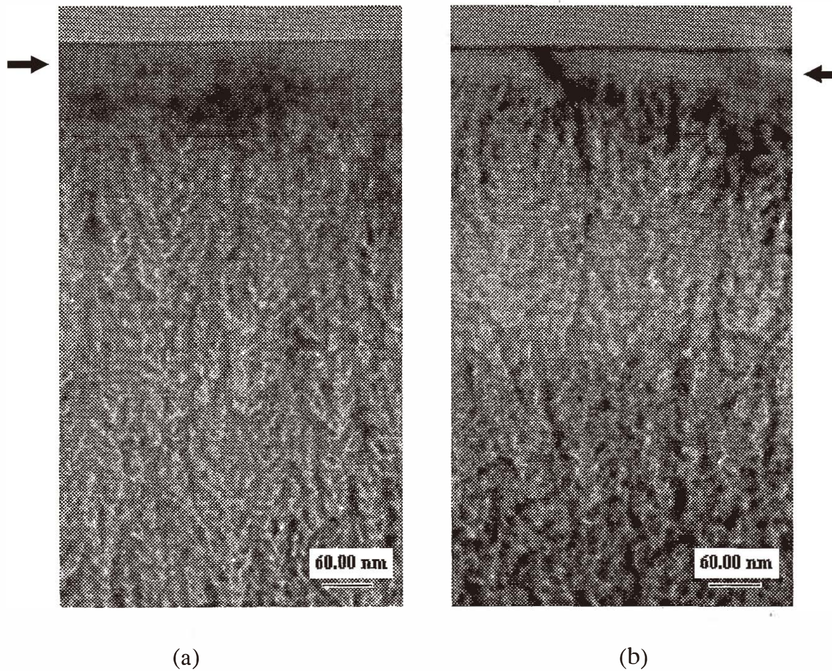

(a) (b)

Fig. 6. TEM cross-sectional image of PS membranes realized on 0.02 Ω·cm p-type silicon, using current density $J = 70$ mA/cm^2 and [HF] = 25% to obtain $p = 55\%$ (a), and $J = 40$ mA/cm^2 and [HF] = 15% to obtain $p = 75\%$ (b). Note that at the top of these two images is a very thin (100 – 200 nm) nonanodized Si layer that rests at the bottom of the PS membrane.

Table 3
Simulated heating power required to maintain a 25-μm-thick insulating membrane at the working temperature of 450°C, while varying residual silicon layer thickness.

Residual Si layer [nm]	0	100	200	300
Heating power [mW]	100	120	140	165

porosity sample (Fig. 7(b)) shows arcing of the diffraction spots, which is typical of highly porous layers.(14)

4.3 *PS passivation and stabilization*

As has been previously discussed, thermal treatment of the PS layer is necessary for passivation and stabilization before it undergoes any further technological processing. In this section, the results related to thermal treatments of the PS layer in an ammonia ambient are presented. A rapid thermal system (RTS) and a standard furnace were used for PS processing in ammonia. To validate the thermal treatment performed on the PS layer, we

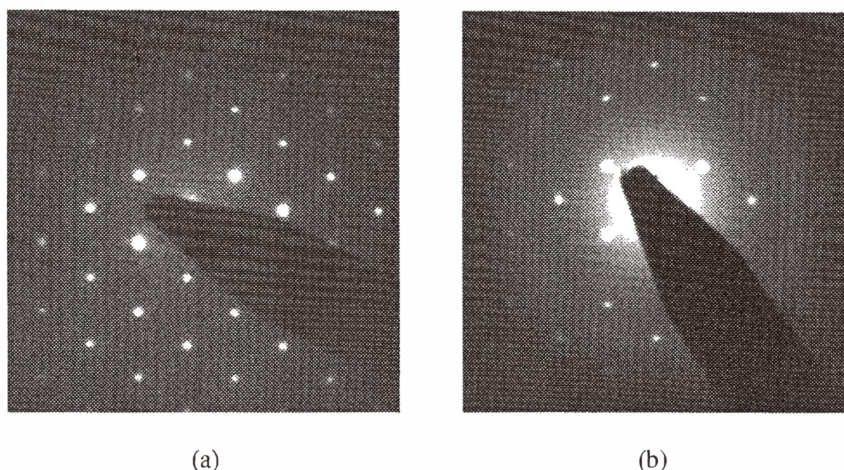

Fig. 7. Electron diffraction patterns of NPS layers in membranes with different porosity values: p = 55% (a) and p = 75% (b).

took into account its effects on: i) wafer and PS membrane warpage, ii) the pronounced blister-like shape of the membrane, and iii) membrane integrity after the thermal treatment. For these tests, square membranes of 1, 1.5, 2, 2.5 mm per sides were realized. Since the passivation process was performed after Si anodization, the effect of the latter step on membrane warpage was also investigated. This was necessary because, as reported by some authors,[15] Si in the PS layer is characterized by a lattice parameter value larger than that of monocrystalline Si. Therefore, the planarity of the PS membrane is expected to change due to volume expansion that occurs as an effect of the difference in lattice parameter. Indeed, this was observed in our membranes when their warpage was measured with respect to that of massive Si surrounding the membrane before and after the anodization process. For the porosity values considered here, namely 55% and 75%, the magnitude of membrane warpage after the anodization process was relatively small for membrane size smaller than 1.5 mm per side, while it was quite large for those of bigger size. No clear evidence of the two porosity values on the membrane warpage was noted.

As far as the PS passivation process in ammonia is concerned, a comparison of the results obtained from the nitridation step performed in a standard furnace or in a RTS have highlighted a completely different trend. While the nitridation step performed in a standard furnace gave results similar to those obtained in the case of PS oxidation, the nitridation step performed in the RTS gave good membrane integrity without increasing the warpage after the anodization step.

4.3.1 *PS ammonia nitridation in a standard furnace*

The nitridation step carried out in a standard furnace starts with an oxidation step performed in dry O_2 at 300°C for 1 h. This step is necessary to prevent coarsening of the PS matrix. After this step, regardless of whether the procedure is carried out in oxygen or in

nitrogen, the PS membranes show a warpage change 4 – 5 times larger than that observed after the anodization step. Then, the temperature is increased to 800°C in N_2 ambient. At this temperature, ammonia is introduced into the quartz tube, then the temperature is raised to 1000°C and nitridation is performed for 30 min. At the end of the process, when the wafer is cooled to room temperature, the PS membranes are either broken or assume a pronounced blister-like shape.

This result can be explained if we consider that by using a standard furnace for the thermal nitridation of PS, it is possible that the air back-streaming from the furnace door increases oxygen and water vapor content inside the quartz tube by 500 – 600 ppm. Despite the relatively small amount of oxygen available in the tube, it could be sufficient, via a very fast surface reaction with Si, to completely oxidize the PS surface rather than to convert Si into Si_3N_4. This behaviour was also confirmed by RBS analysis, which showed the presence of a very large amount of oxygen inside the PS layer (Table 4).

4.3.2 *PS ammonia nitridation in RTS*

The nitridation process executed at 1100°C for 2 min in RTS is performed in such a way that the sealed small reaction chamber of the RTS is abundantly purged with nitrogen before the temperature increase. In this case, the residual oxygen partial pressure inside the reaction chamber is extremely low and Si surface reaction with ammonia prevails. Rapid thermal nitridation of PS is executed while the step at 300°C is not performed; we believe that PS coarsening is prevented first by temperature increase rate (> 125°C/s) and then by the few Si_3N_4 monolayers (~ 3 – 4 nm) formed on the PS walls.

The occurrence of PS nitridation under the reported conditions was investigated by means of the RBS technique. RBS analysis was performed using 2 MeV He^+, and the results are shown in Fig. 8. The samples had 55% and 75% porosity and were exposed to ammonia in RTS at 1100°C using two cycles of 2 min each. In order to analyze the results of the RBS spectra taken from the surface of the NPS layers (simulation data are given in Table 4), it is useful to normalize O and N concentrations to Si concentration, due to

Table 4
Surface chemical composition of the nitrided porous silicon layer as obtained from simulations of data measured with the RBS technique.

Sample	Porosity	PS COMPOSITION(± 2%)				
	%	Si%	O%	N%	O/Si	N/Si
As-prepared PS	55	93	7	—	0.08	—
Air-aged PS	55	83	17	—	0.20	—
OPS (300°C, 1h, O_2)	55	72	28	—	0.39	—
NPS (300°C, 1h, O_2+ 1000°C, 30 min, NH_3)	55	43	45	12	1.04	0.28
NPS (RTN, 1100°C, 4min NH_3)	55	51	16	33	0.31	0.64
NPS (RTN, 1100°C, 4min NH_3)	75	41	22	37	0.53	0.90

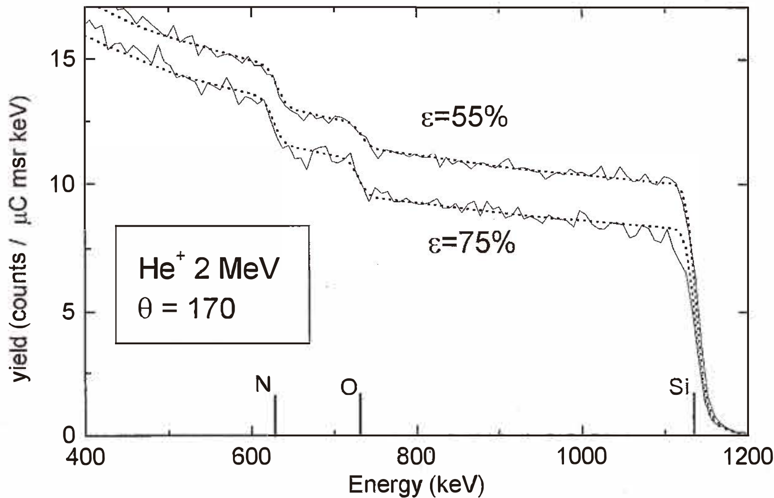

Fig. 8. Experimental (solid lines) and simulated (dotted lines) RBS spectra taken at the surface of NPS membranes (27 μm thick) with different porosity values (55% and 75%).

difference in porosity of the two NPS samples. By changing the porosity from 55% to 75%, O/Si and N/Si ratios increase by 70% and 38%, respectively. These results can be explained if we consider the increase in surface area, related to the increase in porosity from 55% to 75%.

Oxygen concentration in the 55% and 75% PS layers, as evaluated by RBS analysis, was 16% and 22%, respectively. This fairly high concentration of oxygen cannot be attributed only to the formation of native silicon oxide on the PS walls. In fact, the relative oxygen content in samples with RTN treatment is higher than that in a PS sample with 55% porosity and aged for several months (~ 4) in air (Table 4). As has been reported previously,[16] PS can incorporate oxygen during the first steps used to stabilize the PS structure and to purge the chamber, or during nitridation itself, from impurities in the ammonia gas.

To verify the occurrence of an anomalous reaction at 1100°C between ammonia and the PS layer, which might completely transform Si in the rods into SiON, the XRD technique was used to determine the degree of crystallinity of Si in the PS layer after the nitridation process. In this case, thermal treatment at 1100°C performed in two cycles of 2 min each was carried out on 55% and 75% PS layers. XRD analysis showed that even under the heaviest nitridation conditions (2'+ 2' at 1100°C in ammonia ambient), crystalline Si is still present in the PS layer. This result confirms the self-limiting reaction of nitrogen with Si, which was previously observed when a planar Si surface was exposed to ammonia: the very small diffusion coefficient of the nitriding species through the formed SiON limits the thickness of grown SiON to 3 – 4 nm.[17]

Finally, the thermal behaviour of nitrided porous silicon membranes was investigated by means of the photoacoustic (PA) technique. As well known, the PA technique is based on the direct detection of heat generated in a sample as a consequence of nonradiative decaying processes following light absorption. In the conventional experimental arrangement, a sample is enclosed in a cell and exposed to an amplitude-modulated light beam. As a result of periodic heating of the sample, the pressure in the cell oscillates at the modulation frequency and is detected by a sensitive microphone coupled to the cell. In the experiment described here, the two-beam phase-lag method(18) was used. A chopped argon ion laser beam (514 nm) was directed to the opposite side of the sample, and the pressure phase difference was detected. Measurements were made as a function of the modulation frequency in the range of 50 to 400 Hz. All of the investigated membrane samples were obtained from the same wafer, and therefore, they had the same thickness of $27 \pm 1\ \mu m$. As a first approximation, the light absorption coefficient of the sample was assumed to be so high that light absorption was localized to the surface; moreover, possible effects related to the porosity of the material (in particular, expansion/contraction of interstitial gas and effect of light scattering on heat distribution in the sample) were neglected. Under these assumptions, the phase difference was related to the thermal diffusivity of the sample by a simple model,(19) and a best-fit procedure between the experimental data and the theoretical curves allowed the evaluation of the approximate thermal diffusivity value. Therefore, if the density and specific heat of the material are known, thermal conductivity values can be obtained. Figures 9(a) and 9(b) show the phase difference for samples with 55% and 75% porosity, respectively, while in Table 5, the thermal diffusivity values obtained by the best-fit procedure are given. The corresponding thermal conductivities (obtained under the assumption that the specific heat of porous silicon is the same as that of crystalline silicon (0.713 J/g·K), and the density is scaled with respect to that of c-Si (2.32 g/cm^3) as a function of porosity), range from 0.7 W/m·K to 6 W/m·K, in agreement with values reported previously.(4,13,20,21) (The approximations considered allow estimation of thermal conductivity with an error of about 15%).

It is worthwhile to note that the lowest thermal conductivity of the PS material is about half the value reported for SiO_2 (1.4 W/m·K), and in the other cases, it is very close to that of Si_3N_4 (2.25 W/m·K). Therefore, the NPS membranes are very promising for the application we seek. Moreover, from Table 5, we notice that regardless of the nitridation treatment, for samples with 55% porosity, the thermal conductivity of the PS layer is decreased, while for samples with 75% porosity, the thermal conductivity value is increased. This trend can be explained by considering that for membranes with low porosity (55%), the thermal conductivity of Si prevails, and the addition of a passivation layer reduces the total thermal conductivity of the PS layer. In contrast, when the porosity is high (75%), Si constitutes only 25% of the entire layer, while most of the available volume is occupied by air. In this case, the predominant contribution to thermal conductivity is from air, whose thermal conductivity is very low (0.026 W/m·K); therefore, the addition of a passivation layer reduces pore volume and hence air volume, and an overall thermal conductivity increase is observed.

Looking at the data in Table 5, the best treatment in terms of the thermal conductivity value of the PS layer is RTN executed at 1100°C in NH_3 for 2 min. In fact, after this

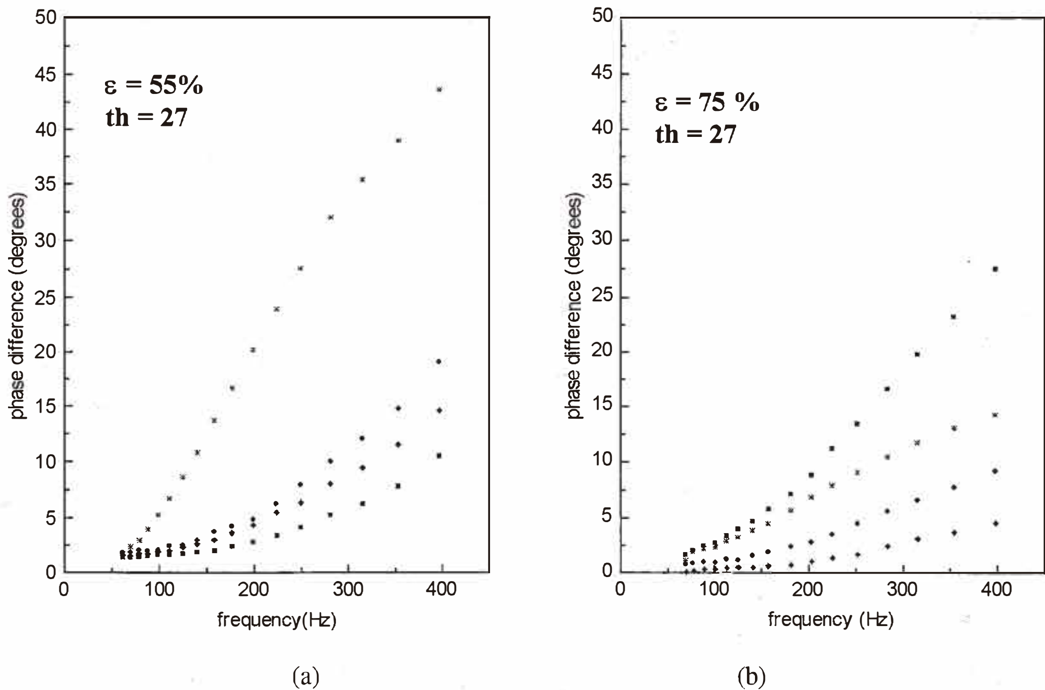

Fig. 9. Phase difference between front and rear illuminations for NPS membranes with 55% porosity (a) and 75% porosity (b). The symbols are described in Table 5.

Table 5
Thermal diffusivity values obtained for NPS suspended membranes, with different porosities and nitrided in RTS under different conditions, fitting data from PA measurements.

Sample name and symbol	Porosity [%]	Preparation procedure	Thermal diffusivity [cm²/s]	Thermal conductivity [W/mK]
197b ■	55	as-prepared PS	0.055	4.09
196b ♦	55	RTN,1000°C, 2’	0.036	2.68
197a *	55	RTN,1100°C, 2’	0.01	0.74
196a ●	55	RTN,1100°C, 2’+2’	0.028	2.08
195b ■	75	as-prepared PS	0.016	0.66
194b ♦	75	RTN,1000°C, 2’	0.16	6.62
195a *	75	RTN,1100°C, 2’	0.04	1.65
194a ●	75	RTN,1100°C, 2’+2’	0.052	2.15

process, the thermal conductivity of PS with 55% porosity reaches the lowest value, while for samples with 75% porosity, this treatment determines the lowest increment. Further investigations are in progress to confirm this result.

5. Conclusions

Thick PS layers were investigated as thermo-insulating materials in place of thin membranes (realized with Si_3N_4, SiC or SiO_2) normally used in silicon microstructures for gas sensor applications. Two different processing technologies were pursued. In both cases, we used a PS layer with a meso-porous structure formed on a heavily doped p-type Si substrate.

In the first approach, the complete conversion of the PS structure into a compact SiO_2 layer was achieved. An optimized thermal oxidation treatment was carried out to completely convert PS into SiO_2, and different techniques (RBS and EDS) confirmed that the stoichiometry of the OPS layer was the same as that of thermal SiO_2. Unfortunately, the wafers containing hundreds of OPS windows exhibited significant wafer warpage, which inhibited the possibility of further processing.

To solve the above problem, another approach was investigated. In this case, PS was nitrided in NH_3 at high temperatures. During this thermal treatment, a thin oxynitride film was grown on the PS pore walls. After the nitridation treatment, the PS structure remained "open," and air filled the pores. Among the different nitridation processes tested, the most suitable was that executed in RTS, which seemed to stabilize the PS structure without warping the PS membrane or the wafer. The thermal behavior of NPS membranes (investigated by means of the PA technique) showed that the thermal conductivity was quite similar to that of SiO_2 or Si_3N_4 layer and was 2 – 2.5 orders of magnitude (according to the nitridation temperature and time used) lower than that of crystalline Si.

In conclusion, the nitridation of PS membranes seems to be challenging for the application we seek. In fact: i) the fabrication process is fully IC compatible, (with the exception of the KOH process step that can be substituted by TMAH); ii) FEM simulations have shown that, at the target temperature of 450°C, power consumption is 140 mW; and iii) the thermal conductivity of NPS membranes, two orders of magnitude lower than that of Si membranes, is comparable to that of thermal SiO_2 or Si_3N_4.

Acknowledgment

We would like to thank A. Garulli for TEM sample preparation. M. Servidori is also acknowledged for X-ray analysis. Finally, we are grateful to F. Corticelli for SEM observation.

References

1 I. George, B. Bonvalot, A. Girard, J. Suski, M. Wagener and A. Zarudiansky: Proc. EUROSENSORS **VIII** (1994) 110.

2 J. S. Suehle, R. E. Cavicchi, M. Gaitan and S. Semancick: IEEE Electron Device Lett. **14** (1993) 118.

3 A. Drost, P. Steiner, H. Moser and W. Lang: Sensors and Material **7** (1995) 111.
4 V. Labunov, V. Bondarenko, L. Glinenko, A. Dorofeev and L. Tabulina: Thin Solid Film **137** (1986) 123.
5 R. Herino, A. Perio, K. Barla and G. Bomchil: Mat. Let. **2** (1984) 519.
6 J. G. Korvink: The SOLIDIS User's Manual: Version 1.0, PEL-ETH Zurich (1995).
7 O. Tabata: IEEE Trans. Electron Dev. ED-**33** (1986) 361.
8 W. Lang: Mat. Science & Eng. R (1996) R17.
9 S. Barrett, F. Gaspard, R. Herino, M. Ligeon, F. Müller and I. Ronga: Sensors and Actuators A **33** (1992) 19.
10 J. J. Yon, K. Barla, R. Herino and G. Bomchil: J. Appl. Phys. **62** (1987) 1042.
11 P. Maccagnani, R. Angelucci, P. Pozzi, A. Poggi, L.Dori, G. C. Cardinali and P. Negrini: Sensors and Actuators B **49** (1998) 22.
12 K. Barla, R. Herino and G. Bomchil: J. Appl. Phys. **59** (1986) 439.
13 G. Benedetto, L. Boarino and R. Spagnolo: Appl. Phys. A **64** (1997) 155.
14 A. G. Cullis and L. T. Canham: Nature **353** (1991) 335.
15 K. Barla, R. Herino, G. Bomchil and J. C. Pfister: J. of Crystal Growth **68** (1984) 727.
16 S. S. Tsao, T. R. Guilinger, M. J. Kelly, H. J. Stein, J. C. Barbour and J. A. Knapp: J. Appl. Phys. **67** (1990) 3842.
17 S. P. Murarka, C. C. Chang and A. C. Adams: J. Electrochem. Soc.: Solid-State Science and Technology **126** (1979) 996.
18 O. Pessoa Jr., C. L. Cesar, N. A. Patel and H. Vargas: J. Appl. Phys. **59** (1986) 1316.
19 P. Charpentier and F. Lepoutre: J. Appl. Phys. **53** (1982) 608.
20 G. Amato, G. Benedetto, L. Boarino, N. Brunetto and R. Spagnolo: Opt. Eng. **36** (1997) 423.
21 G. Gesele, J. Linsmeier, V. Drach, J. Fricke and R. Arens-Fischer: J. Phys. **30** (1997) 2911.